Integrated Simulations and Respective Simulation Modeling for FIREX-I

H. Sakagami 1), T. Nakamura 2), T. Johzaki 3), H. Nagatomo 3), Y. Nakao 4), T. Taguchi 5), K. Mima 3)

1) Department of Simulation Science, National Institute for Fusion Science, Toki, Japan
2) Japan Atomic Energy Agency, Kyoto, Japan
3) Institute of Laser Engineering, Osaka University, Osaka, Japan
4) Dept. of Applied Quantum Phys. and Nuclear Eng., Kyushu University, Fukuoka, Japan
5) Department of Electrical and Electronic Engineering, Setsunan University, Osaka, Japan

e-mail contact of main author: sakagami.hitoshi@nifs.ac.jp.

Abstract. Integrated simulations for the fast ignition with a cone-guided target and 10[ps] heating laser have been performed to investigate the core heating property of FIREX-I experiments. It was found that the core reached higher average temperature when the preformed plasma on an inner surface of the cone tip had longer scale length. As the scale length of the preformed plasma was not easily controllable, a low-density foam coated target was proposed to prevent the reduction of the fast electron beam intensity during the laser irradiation. Optimum foam density and thickness were estimated by averaged core temperatures calculated by the integrated simulations. As respective simulation modeling, the cone angle and the laser spot size were optimized by 2D relativistic PIC simulations and a double-cone design was suggested. Simulations for 2D cone-guided non-spherical implosion were performed by the radiation-hydro code to preliminarily design targets, and the core heating simulations were performed by the relativistic Fokker-Planck code to estimate the magnetic field effect on the core heating.

1. Introduction

It was reported that the fuel core was heated up to ~ 0.8[keV] in the fast ignition experiments with cone-guided targets at Osaka University (FI02) [1], but efficient heating mechanisms and achievement of such high temperature have not been clarified yet. To attack this challenging problem, we have been promoting the Fast Ignition Integrated Interconnecting code (FI^3) project [2]. Under this project, the radiation-hydro code (PINOCO), the PIC code (FISCOF), and the relativistic Fokker-Planck code (FIBMET) are integrated with data exchanges to understand overall complicated physics in the fast ignition. According to FI^3 integrated simulations for the FI02 experiments, it was found that the density gradient of preformed plasma, which is produced by pre-pulse of the laser at an inner surface of the cone tip, strongly affects a generation mechanism of fast electrons, hence efficiency of core heating. With increases in the scale length (L_f) of preformed plasma from 0 to 1.5[μm], the energy coupling from the heating laser to fast electrons becomes large, so that the deposited energy and the resultant core ion temperature increase. When L_f becomes long furthermore, the total beam energy of fast electrons gradually decreases. However, the higher energy component (E>2[MeV]) increases, and then the lower energy component (E<2[MeV]) that is much effective for core heating, decreases faster than the total beam energy. As the result, the deposited energy in the fuel and the core ion temperature decrease. The optimum L_f for core heating is found to be 1.5[μm] under these conditions. In this situation, the energy coupling from the heating laser to the core is 14.9[%] and ion in the core is heated up to 0.86[keV], which is comparable to the value obtained in experiments [3].

The FIREX-I project aims at demonstrating that the imploded core can be heated up to the ignition temperature, 5[keV]. Experimental conditions are much different from those in the FI02 experiments, and we should not only perform the integrated simulations but also model

the respective physics to evaluate the performance of the fast ignition prior to FIREX-I experiments.

2. Integrated Simulations for FIREX-I

The heating laser in FIREX-I is designed to have the total energy of 10[kJ] but to retain the same intensity in the FI02 experiments because higher intensity generates faster electrons that cannot heat the core efficiently. So the pulse duration is set up to be 10[ps] instead of 750[fs] in FI02. The 10[ps] pulse length is long enough even for heavy Au preformed plasma of the cone to be pushed and compressed by the ponderomotive force. The laser-plasma interaction is much affected by deformation of the preformed plasma. There have been, however, few researches using such a long pulse laser. Thus we have investigated fast ignition physics for 10[ps] heating laser with the use of FI^3.

2.1. Scale Length of Preformed Plasma

When the heating laser irradiates the preformed plasma, the profile steepening occurs and the electron density is locally maximized at the laser front. As the heating laser directly interacts with the sharp edge overdense plasma, fast electrons are mainly generated by the longitudinal ponderomotive force. The longitudinal ponderomotive force on electrons is given by a following equation [4].

$$f_p = -\frac{\partial}{\partial x}\left(\frac{m v_{osc}^2}{2} \frac{4\omega_L^2}{\omega_{pe}^2} e^{-2\omega_{pe}x/c} \left[\frac{1+\cos 2\omega_L t}{2} \right] \right) \propto \left(\frac{v_{osc}^2}{c^2} \right) \omega_L^2 \left(\frac{c}{\omega_{pe}} \right) \qquad (1)$$

The magnitude of the force is proportional to c/ω_{pe}, namely $n_e^{-1/2}$. As intensity is obtained by multiplying a force by a velocity, the beam intensity of fast electrons that are generated by the longitudinal ponderomotive force can be estimated by multiplying f_p by the velocity. Because the laser intensity is relativistic, the velocity of fast electrons can be assumed to be a light speed. Thus the fast electron beam intensity would be proportional to f_p, hence to the inverse square root of the electron density. While the electron density goes up, less fast electrons are generated by the weakened ponderomotive force and the beam intensity is also reduced. Fast electron beam intensity as a function of bulk electron density at the interaction front is shown in FIG.1 for L_f=1, 2, 3, 5 and 10[μm]. Each plot point is corresponding to different observation times. As the underdense plasma is swept away from the laser-plasma interaction

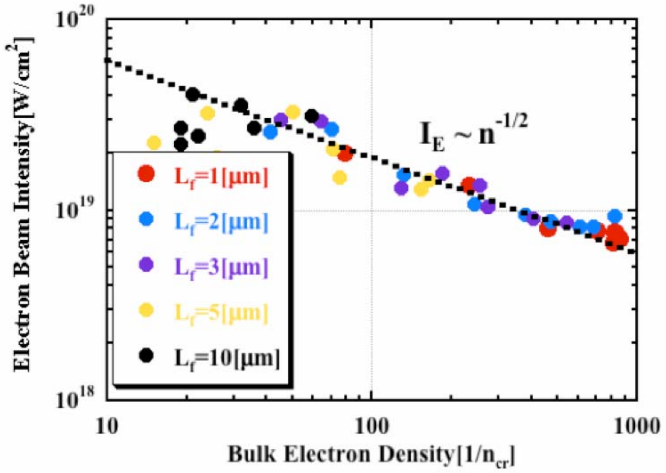

FIG.1. Fast electron beam intensity as a function of bulk electron density. Colors of red, blue, purple, yellow and black indicate L_f=1, 2, 3, 5 and 10[μm], respectively.

region and the laser directly irradiates the snowplowed plasma, the beam intensity well scales as the inverse square root of the electron density independent of the scale length of the preformed plasma [5].

Ref.6 also discussed about the hot electron beam intensity scaling. They conclude that the beam intensity is obtained by multiplying hot electron energy (hot electron temperature), hot electron density and a velocity. While the energy (temperature) and density are proportional to $n_e^{-1/2}$ and $n_e^{1/2}$ respectively, the intensity tends to stay constant because the velocity is also constant, a light speed. Thus there is a large discrepancy with our results in the intensity scaling. To compare details, we observed the hot electron temperature and density in our simulations for L_f=1, 5 and 10[μm] and plotted them as a function of bulk electron density in FIG.2 (a) and (b). Hot electron temperatures are calculated as a slope temperature for a lower part (0.4 ~ 1[MeV]) and a higher part (1 ~ 3[MeV]) because the slope temperature cannot be represented by one temperature. Hot electron density is calculated by counting up the number of electrons whose energy is higher that 100[keV]. Each plot point is also corresponding to different observation times.

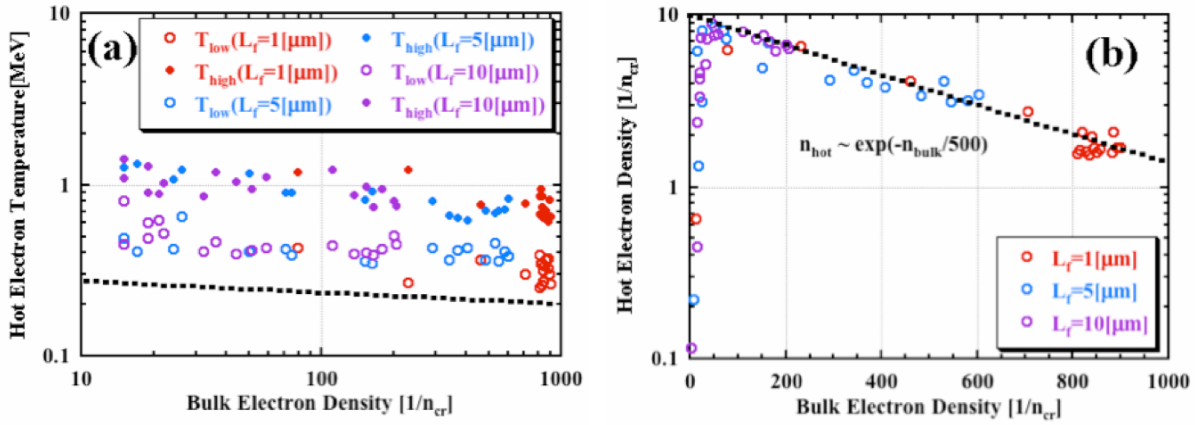

FIG.2. (a) Hot electron temperatures as a function of bulk electron density. Open and solid circles indicate a lower and higher hot electron temperatures, respectively. (b) Hot electron density as a function of bulk electron density. In both figures, colors of red, blue and purple indicate L_f=1, 5 and 10[μm], respectively.

In our results, the hot electron temperature tends to stay constant, and the hot electron density decreases with increasing the bulk electron density, not proportional to $n_e^{1/2}$ at all. These disagreements mainly come from different observation methods in simulations. We observe hot electron characteristics based on the hot electron flux, namely we count up electrons that get across the observation point from the laser-plasma interaction region to the core, but they count up all electrons in the observation region. Another difference is that their results come from only one snapshot just after the preformed plasma blown away, but we track time history data of hot electrons. In addition, they ignored the density increment of the cone due to compression by the ponderomotive force. We believe that the flux-based observation method is more accurate to catch features of the fast electron beam, and the scaling law of fast electron beam intensity to the electron density is proportional to $n_e^{-1/2}$, not constant.

We have performed FI^3 integrated simulations in such conditions with different L_f and evaluate the core temperature. In the case of short L_f, the average core temperature quickly rises but shortly saturates because the preformed plasma is snowplowed and the electron density increases; consequently fast electron beam intensity decreases according to the scaling law. In the long L_f case, the beam intensity is maintained and the core heating is sustained for

a long time, thus the core reaches higher average temperature [5]. It is emphasized that the characteristic of the dependence of core heating on L_f of the preformed plasma in long pulse lasers is completely different from that in short pulse lasers [3].

2.2 Low Density Foam

The core heating properties in the fast ignition are affected by the characteristics of the preformed plasma, which is generated by a pre-pulse of the heating laser, but the pre-pulse is nature of the laser device itself and is not easily controllable. To control the preformed plasma density, we propose to coat an inner surface of the cone target with low-density foam materials, such as aerogel, which are fully ionized by a low intensity pre-pulse. We can prevent the preformed plasma from being snowplowed to extremely high density at the laser front, and expect that the fast electron beam intensity is kept at the high level during laser irradiation.

We set up the heating laser to $I_L=10^{20}$[W/cm^2], λ_L=1.06[μm], τ_{rise}=375[fs], τ_{flat}=10[ps] and τ_{fall}=375[fs], and the Au cone tip to 500n_{cr}, real mass, Z=30, 10[μm] flattop plasma. We put the foam plasma (SiO_2 aerogel, A=20, Z=10, 40[μm] thickness) with different densities (n_{foam}) in front of the Au cone tip plasma and the CD plasma (500n_{cr}, A=7, Z=3.5, 50[μm] thickness) behind it. The fast electron beam is observed at the 10 [μm] rear point of the Au-CD boundary. Time evolutions of fast electron beam intensity and time averaged fast electron energy spectrum for n_{foam}=2, 5, 10, 20, 30 and 50n_{cr} are shown in FIG.3 (a) and (b), respectively. As intensity of the heating laser is 10^{20}[W/cm^2] and fast electron beam intensity is around 4×10^{19}[W/cm^2] at the maximum level, the instantaneous energy conversion rate from laser to electron can be roughly estimated as 40%. If the density of the foam plasma is below the relativistic critical density (case $n_{foam}=2n_{cr}$), the heating laser can penetrate into the foam plasma and directly interact with the extreme overdense Au plasma after 2[ps]. After that, the fast electron beam intensity is quickly reduced and fast electrons cannot be generated so much. In the case of $n_{foam}=5n_{cr}$, the foam density is also relativistically underdense, but the rising time of the laser is long enough to compress the foam plasma higher than the relativistic critical density before the laser reaches the peak intensity. So the laser cannot penetrate into the foam plasma. The fast electron beam intensity is sustained at the nearly peak level until 4, 5 and 7[ps] with cases of n_{foam}=5, 10 and 20n_{cr} because the electron density at the interaction region does not increase so much. After that time, the foam plasma is completely plunged into

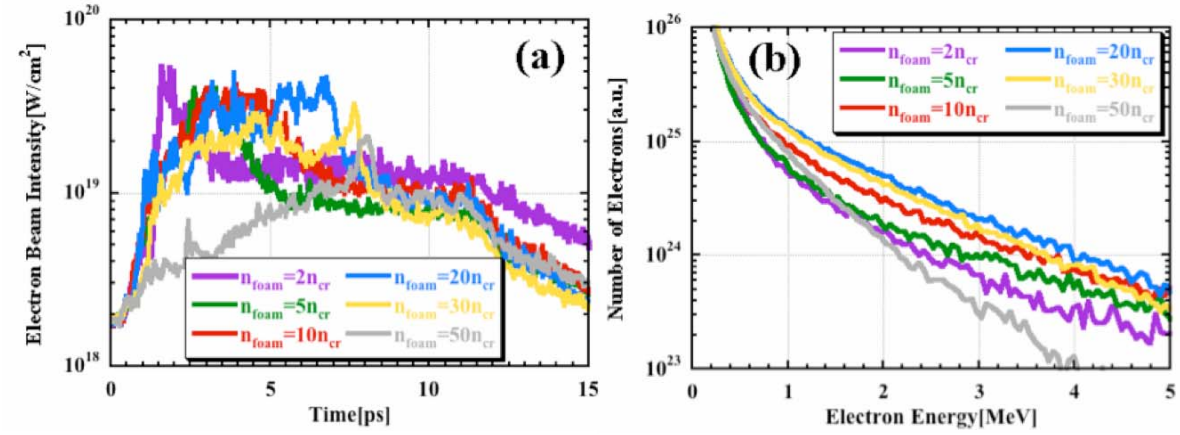

FIG.3. (a) Time evolutions of fast electron beam intensity and (b) time averaged fast electron energy spectrum. In both figures, colors of purple, green, red, blue, yellow and gray indicate the foam density of 2, 5, 10, 20 30 and 50n_{cr}, respectively.

the Au plasma. Therefore the heating laser has to directly interact with the extreme overdense Au plasma like the case of $n_{foam}=2n_{cr}$, and it results in reduction of the fast electron beam intensity. Among there cases, much fast electrons whose energy is efficient for core heating are generated in the case of $n_{foam}=20n_{cr}$. Appropriate fast electrons are also generated with the case of $n_{foam}=30n_{cr}$, but the beam intensity is lower than that of the $n_{foam}=20n_{cr}$ case due to higher foam density. On the other hand, when the foam density is high enough (case $n_{foam}=50n_{cr}$), electrons in the foam plasma are snowplowed at the laser front to such density that the fast electron beam intensity can be substantially repressed at a low level, and the fast electron slope temperature is also low from the beginning. The beam intensity is dropping after 12[ps] when the laser irradiation is turned off.

To prevent the foam plasma from being swept away during irradiation of the heating laser, we put the thicker foam plasma, and the drop-off time of the beam intensity is found to be successfully extended according to the thickness. The total fast electron beam energies that are calculated by integrating the beam intensities as a function of the foam density are shown in FIG.4 (a) for different foam thicknesses, 40, 60, 70 and 80[μm]. For $n_{foam}=20$ and $30n_{cr}$ cases, 60[μm] thickness seems to be enough to prevent the depletion, but 80[μm] is required in the case of $n_{foam}=10n_{cr}$ and much more thickness is needed for $n_{foam}=5n_{cr}$ case. The recession velocity of the foam plasma can be estimated by balancing the momentum flux of the mass flow with the laser pressure, given by a following equation [7].

$$\frac{u}{c}=\sqrt{\frac{n_{cr}}{2n_e}\frac{Zm}{M}\frac{I\lambda^2}{1.38\times10^{18}}} \qquad (2)$$

The minimum thickness of the foam plasma can be also estimated by multiplying the recession velocity by the laser irradiation period, 10[ps], and is given by 133, 94, 66 and 54[μm] for $n_{foam}=5$, 10, 20, and $30n_{cr}$, respectively. This estimation has a good agreement with the total beam energy in FIG.4 (a). As the core heating is greatly affected by not only the beam intensity but also the energy spectrum of fast electrons, hence the foam density, we have performed FI^3 integrated simulations to estimate core temperatures. Maximum core electron temperatures, which are averaged over the dense region (ρ>10[g/cm^3]), as a function of the foam density for different thicknesses are shown in FIG.4 (b). The total fast electron beam energy for case ($10n_{cr}$, 80[μm]) is almost same as that for case ($20n_{cr}$, 60[μm]), but the maximum averaged core electron temperature in the case of ($20n_{cr}$, 60[μm]) is higher that that

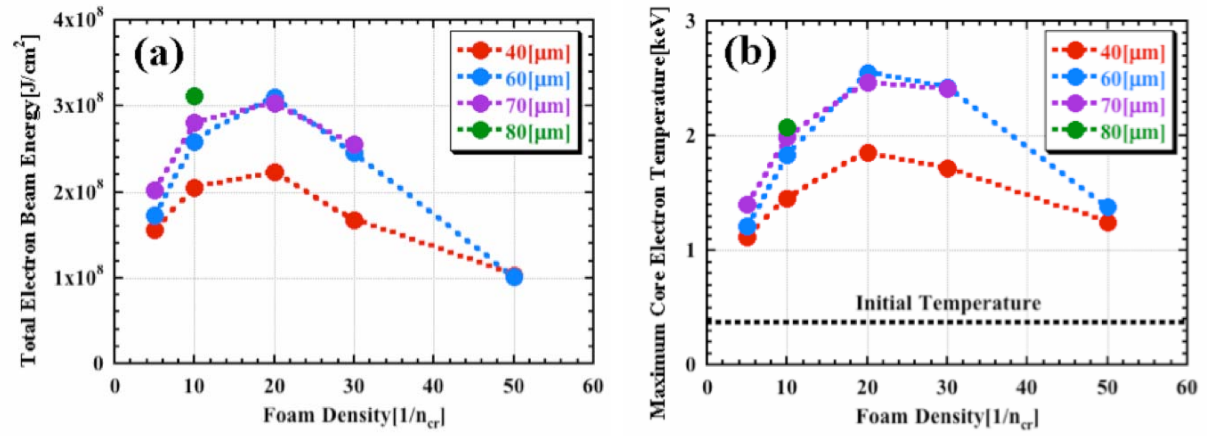

FIG.4. (a) Total fast electron beam energy and (b) maximum averaged core electron temperature. In both figures, colors of red, blue, purple and green indicate the foam thickness of 40, 60, 70 and 80[μm], respectively.

of ($10n_{cr}$, 80[μm]) because fast electrons with ($20n_{cr}$, 60[μm]) foam are more suitable for core heating than those with ($10n_{cr}$, 80[μm]) foam. (*see FIG.3 (b)*)

To avoid the heating laser anomalously penetrating into the foam plasma, the density of the foam should be higher than that of the relativistic critical density, namely $8.6n_{cr}$ for $I_L=10^{20}$[W/cm^2]. The density of the foam should be also low enough to prevent electrons in the foam plasma from being snowplowed to extremely high density at the laser front, namely $50n_{cr}$ for current conditions in this paper. The foam plasma should also be so thick to stay there until the heating laser is turned off, and lower density requires thicker coat. But the thick foam plasma leads to less efficient heating due to a long travel distance of fast electrons to the core. Thus the optimum foam density and thickness for core heating may exist. Under these parameters, the averaged core electron temperature can reach 2.6[keV] with $20n_{cr}$, 60[μm] thickness foam. We can conclude that we can appropriately control the fast electron generation for core heating with the low-density foam coated on cone targets.

3. Respective Simulation Modeling

First respective simulation modeling is the geometry optimization of the cone shape for FIREX-I. The dependence of the electron energy characteristics on the cone angle and the laser spot size is investigated with 2D FISCOF simulations. The energy absorption rate increases with decreasing the cone angle, because the coupling of the laser to the cone side wall is enhanced and the irradiation amplitude at the cone tip is intensified as the cone angle reduces. The sharper cone, however, causes larger angle of laser irradiation onto the side wall, and it leads to less effective interaction between the laser and the plasma. It is also found that the electron effective temperature becomes higher with decreasing the cone angle. Together with the absorption rate dependence on the angle, the number of electrons around 1[MeV], which play a crucial role in core heating, are most effectively generated in the 30° cone. As a result, the optimum cone angle is about 30° which realizes a higher energy absorption rate and moderates fast electron energy. The laser spot size determines the laser intensification at the cone tip and how much the interaction at the cone side wall is utilized in generating high-energy electrons, so it is another parameter to be optimized. Since the dominant electron acceleration takes place at the cone tip, the laser diameter should be small enough to deliver the laser energy to the cone tip. On the other hand, when the spot size is smaller than the tip size, the absorption rate decreases because the laser light does not interact with the cone side wall and only hits the tip, which is the same as the plane target irradiation. It is found that the laser energy should not be tightly focused to the tip by the optical lens, but focused to a diameter of about 3-4 times larger than the tip size and utilize the interaction at the cone side wall as well as the cone tip. Although the dominant electron acceleration takes place at the cone tip, interaction at the cone side wall enhances the energy coupling which is an advantage of using cone targets. In addition, a double-cone design is suggested to enhance the fast electron flow to the core. According to PINOCO simulations, the cone target is surrounded by corona plasmas generated by the implosion of a fuel capsule whose density is well above the critical density. In such case, fast electrons generated at the cone side wall propagate freely into the surrounding corona plasma and the energy flux to the core decreases. In order to prevent fast electrons from escaping aside, a double-cone target is introduced. In the double-cone target, the outer cone isolates the side wall of the inner cone, where the laser is injected, from the corona plasma. Therefore, fast electrons are confined inside the inner cone due to the sheath field. The energy distributions of electrons with energies between $0.5<E[MeV]< 2$ of the single cone and the double cone are plotted in FIG.5 (a) and (b), respectively. It is clearly

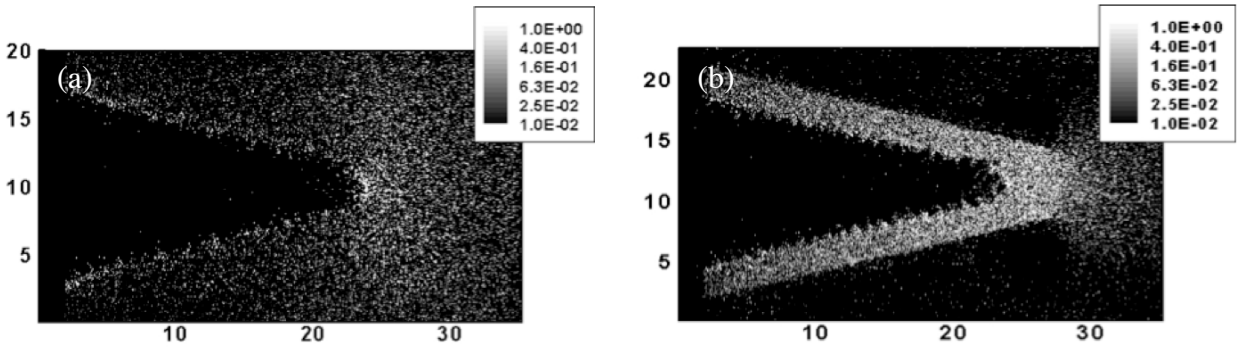

FIG.5.Electron energy density distributions with 0.5<E[MeV]<2 for (a) the single-cone and (b) the double-cone. The energy density is normalized by mc^2n_{cr}.

seen that electrons are confined inside the inner cone of the double-cone target, and it is found that the energy flux of the double cone is 1.7 times larger than that of the single cone [8].

Simulations for 2D cone-guided non-spherical implosion are performed by PINOCO to preliminarily design targets as the second modeling. The dynamics of a non-spherical implosion must be controlled to assemble both high density and high areal density. It is found that the implosion must be finished before the ablated plasma from the cone affects the dynamics of imploding shell [9]. Since the radiation irradiates the cone surface and then ablates the plasma, it also affects the implosion dynamics of the shell. CH coating on the cone, which tamps the gold plasma, is effective to improve the implosion performance [10].

Finally, the core heating simulations are performed by FIBMET. In simulations, we assumed uniformly compressed spherical plasma that has the Gaussian density profile (the density at the center is 200[g/cm^3] and r_{HWHM} is 10[μm]) and the uniform temperature profile both for ions and electrons (T_e=T_i=0.4[keV]). The fast electron beam, which is the super Gaussian in radial direction (the beam intensity at the center is 5.7x10^{19}[W/cm^2], r_{HWHM} is 15[μm]), flat pulse (the duration is 10[ps]) and has the slope temperature of 1[MeV], is artificially injected at the point 50[μm] away from the core center. The spatial profiles of magnetic field (top left), heating rate (top right), bulk electron temperature (bottom left) and ion temperature (bottom right) are shown in FIG.6 for (a) t=1.5[ps] and (b) 4.5 [ps]. In early stage (t<2.3[ps]), the fast electron beam is naturally pinched by the magnetic fields that are self-generated around the beam edge. The core heating is nearly uniform and the heating rate increases due to the beam pinching. After that, the fast electron beam breaks into some filaments and the core heating spots are also spread. On the other hand, the large spatial gradient of bulk electron temperature is induced on the rim of the core because of the fast electron heating. Since this gradient is not parallel to the density gradient, the magnetic field is generated by the thermo-electric force around the rim region and fast electrons are scattered away from the dense core, hence the core heating rate decreases. In late stage (t>5[ps]), the core is heated by the beam component remaining around the beam centre and the heating rate is nearly constant. The magnetic fields are found to affect core heating not directly but though the beam transport in the comparatively low dense region surrounding the dense core center [11].

4. Summary

We propose a cone target, of which an inner surface is coated with a low-density foam, to maintain the fast electron beam intensity at the high level during 10[ps] laser irradiation. FI^3 integrated simulations are performed to estimate core temperatures, and the foam density and

thickness are optimized. As respective simulation modelling, we optimize the cone angle and the laser spot size for FIREX-I by 2D FISCOF simulations and suggest a double-cone design to enhance the fast electron flow to the core. We also perform PINOCO simulations for 2D cone-guided non-spherical implosion to preliminarily design targets, and the core heating simulations with FIBMET to estimate the magnetic field effect on the core heating. Those results are used to design the advanced cone-guided target for FIREX-I [12].

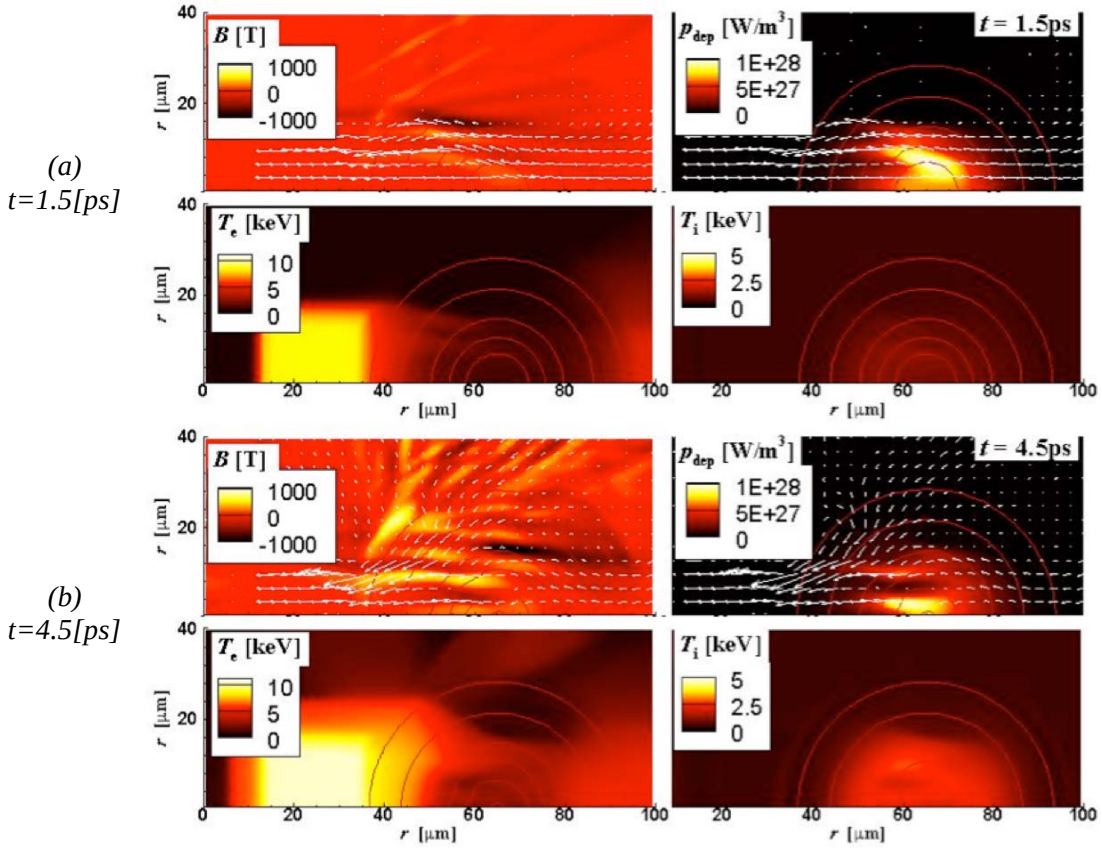

FIG.6. The spatial profiles of magnetic field (top left), heating rate (top right), bulk electron temperature (bottom left) and ion temperature (bottom right).

This work was supported by MEXT, a Grant-in-Aid for Creative Scientific Research (15GS0214).

References

[1] R. Kodama et al., Nature **418**, 933-934 (2002).
[2] H. Sakagami et al., Laser Part. Beams **24**, 191-198 (2006).
[3] T. Johzaki et al., Laser Part. Beams **25**, 621-629 (2007).
[4] S. C. Wilks and W. L. Kruer, IEEE J. Quantum Electronics **33**, 1954-1968 (1997).
[5] H. Sakagami et al., J. Phys.: Conf. Series **112**, 022070 (2008).
[6] B. Chrisman et al., Phys. Plasmas **15**, 056309 (2008).
[7] S. C. Wilks et al., Phys. Rev. Lett. **69**, 1383-1386 (1992).
[8] T. Nakamura et al., Phys. Plasmas **14**, 103105 (2007).
[9] H. Nagatomo et al., Phys. Plasmas **14**, 056303 (2007).
[10] H. Nagatomo et al., IAEA-CN165/IF/P7-18 (2008).
[11] T. Johzaki et al., J. Phys.: Conf. Series **112**, 022054 (2008).
[12] H. Azechi et al., IAEA-CN165/OV/4-1 (2008).